

# What and Whence 1I/‘Oumuamua: A Contact Binary from the Debris of a Young Planetary System?

E. Gaidos<sup>1</sup>

<sup>1</sup>*Department of Geology & Geophysics, University of Hawaii at Mānoa, Honolulu, Hawaii 96822 USA*

Submitted to MNRAS

## ABSTRACT

The first confirmed interstellar interloper in our Solar System, 1I/‘Oumuamua, is likely to be a minor body ejected from another star, but its brief flyby and faintness made it difficult to study. Two remarkable properties are its large (up to 2.5 mag) rotational variability and its motion relative to the Sun before encounter. The former suggests an extremely elongated shape (aspect ratio  $\geq 10$ ) and the latter an origin from the protoplanetary disk of a young star in a nearby association. Against expectations, it is also not comet-like. 1I/‘Oumuamua’s variability can also be explained if it is a contact binary composed of near-equilibrium ellipsoidal components and heterogeneous surfaces, i.e. brighter, dust-mantled inner-facing hemispheres and darker, dust-free outer-facing poles. Such shapes are a plausible outcome of radiation, tides and collisions in systems where planets are clearing planetesimal disks. The probability that 1I/‘Oumuamua has the same motion as a young ( $\lesssim 100$  Myr) stellar association by coincidence is  $< 1\%$ . If it is young, its detection vs. more numerous, older counterparts could be explained as a selection effect due to darkening of surfaces by Galactic cosmic rays and loss of dust. 1I/‘Oumuamua’s apparent lack of ices can be explained if ejected rocky planetesimals are characteristically smaller and thus far more numerous than their icy counterparts: the Solar System may currently host several such objects captured by the combined gravity of Jupiter and the Sun.

**Key words:** minor planets, asteroids: general — minor planets, asteroids: meteoroids — stars: planetary systems — stars: protoplanetary disks — Galaxy: open clusters and associations — ISM: cosmic rays

## 1 INTRODUCTION

We have two windows on the formation and early evolution of planets; the study of meteorites and asteroids in our Solar System, some of which are fragments of primitive bodies that escaped incorporation into planets, and observations of circumstellar disks around young stars in which planets are, presumably, forming by aggregation of solids. Through the former window, we can study relatively primitive protoplanetary material up close and determine the timing of some events; however the processes by which these materials are altered and accreted into planets are not directly observed, nor are we certain this is an unbiased sample of protoplanetary material. Through the latter window, we observe the formation of disks and the coagulation of dust grains, as well as the final products (exoplanets), but most intermediate steps are obscured because the largest objects, containing most of the mass, make the smallest contribution to emitting surface area; some steps could also occur too rapidly to be represented. Data on the solid body population of young

planetary systems is key to understanding their formation and the initial and environmental conditions that control outcomes.

1I/‘Oumuamua (alias A1/2017 U1) is the first small body discovered with an unambiguously hyperbolic and hence unbound orbit *before* entering the Solar System. It was discovered in Pan-STARRS images after perihelion and soon after its closest approach to Earth, recovered in images taken earlier by the Catalina Sky Survey, and monitored for orbit and lightcurve determination by telescopes worldwide (Meech et al. 2017). 1I/‘Oumuamua lacked a coma and thus near-surface ices, but its reddish color is consistent with low-albedo asteroids and comets (Meech et al. 2017; Jewitt et al. 2017; Ye et al. 2017; Bannister et al. 2017; Bolin et al. 2017; Fitzsimmons et al. 2017; Drahus et al. 2017). It is  $\sim 200$  m in size assuming a low albedo.

Probably its most remarkable property besides its orbit is its 2-2.5 magnitudes of apparent photometric variability (uncorrected for phase effects), presumably due to rotation ( $\approx 7$ -8 hr) of a non-spherical shape (Meech et al.

arXiv:1712.06721v2 [astro-ph.EP] 15 Apr 2018

2017; Jewitt et al. 2017; Knight et al. 2017; Bannister et al. 2017; Drahus et al. 2017). An ellipsoidal body (semi-axes  $a$ ,  $b$ ,  $c$ ) with a uniform surface rotating around its shortest ( $c$ ) axis typically produces a light curve that varies approximately as  $a/b$ ; less if viewed nearly pole-on. This has led to the deduction that the aspect ratio of 1I/‘Oumuamua is at least 10:1 (Meech et al. 2017), although Fraser et al. (2017) points out the phase-angle effects could reduce this value. No known body in the Solar System has such an extreme shape, and it requires that 1I/‘Oumuamua has a small but non-zero cohesive strength.

Among Solar System minor bodies with the largest photometric variability are contact binaries where, at certain viewing geometries, one component occults and/or eclipses (shadows) the other. These eclipses produce characteristic cusp-like minima in the lightcurves like that seen in photometry of 1I/‘Oumuamua. Binaries, including contact binaries and “dumb-bell” shapes, occur in all minor body populations of the Solar System (Walsh & Jacobson 2015). A binary configuration, if confirmed, has implications for the size, internal properties and history of this object.

Another remarkable property of 1I/‘Oumuamua is its pre-encounter velocity, which is within a few  $\text{km s}^{-1}$  of groups of nearby young ( $\lesssim 100$  Myr) stars (Young Moving Groups or Stellar Associations), and not too different from the Local Standard of Rest. This further solidifies 1I/‘Oumuamua’s extrasolar origin (Mamajek 2017) and raises the possibility that it is an ejected planetesimal from a young star system (Gaidos et al. 2017), and thus a representative of a population of planetary building-blocks not observationally accessible by other means. (See Hansen & Zuckerman (2017) and Rafikov (2018) for an alternative origin around a white dwarf). Here, I examine the rotation, shape, surface, and origin of 1I/‘Oumuamua in this context, and discuss the implications of its properties for its formation, age, and the parent population of ejected objects.

## 2 ROTATION AND SHAPE

To revisit the question of 1I/‘Oumuamua’s rotation and shape, photometric data of 1I/‘Oumuamua were compiled from Meech et al. (2017), Jewitt et al. (2017), Knight et al. (2017), and Bannister et al. (2017). Apparent magnitudes in Jewitt et al. (2017), Knight et al. (2017), and Bannister et al. (2017) were corrected for differences in solar illumination and distance changes relative to October 25.0 using the JPL Horizons calculator. Magnitudes from those latter sources were converted to  $g$ -band using the colors estimated by those works; conversion (back) to the Sloan from the Cousins photometry reported by Jewitt et al. (2017) used the transformations of Jordi et al. (2006).

The two highest peaks in the Lomb-Scargle periodogram (Scargle 1982) of the entire data set (Fig. 1) are at 3.20 and 3.64 hr. For rotation of a non-spherical shape, the most prominent signal is interpreted as one half the rotation period, in this case 6.40 and 7.29 hr. The latter peak is very close to the period identified by Meech et al. (2017). However, sampling at an interval  $S$  can produce alias signals at  $1/(1/P \pm 1/S)$  and for ground-based observations

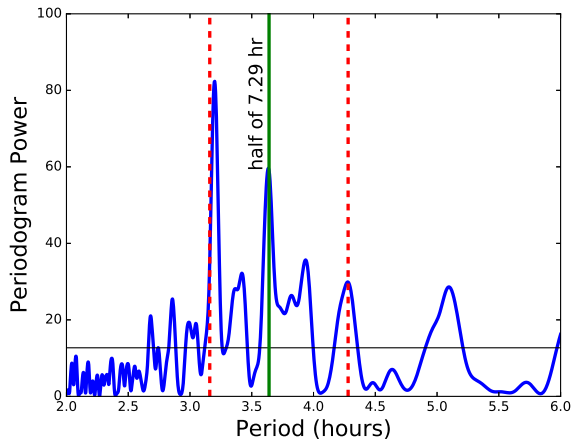


**Figure 1.** Lomb-Scargle periodogram of the combined photometry of Meech et al. (2017), Jewitt et al. (2017), Knight et al. (2017) and Bannister et al. (2017). The green line denotes the period close to that identified by Meech et al. (2017). The red dashed lines mark the alias signals produced by 24 hr sampling.

with  $S = 24$  hr, at least one of the peaks could be an alias (Fig. 1).

Moreover, the phased data reveal inconsistencies between the periodicity at earlier and later times. Fig 2 shows a running periodogram computed with a moving window having a width that is adjusted to always include 100 data points. The time assigned to each periodogram is the mean time of the data in the window. A consistent pattern before relative  $\Delta\text{JD} = 2$  (“early”) is replaced by a different pattern after  $\Delta\text{JD} = 2.7$  (“late”). At intermediate times, the data cannot be explained by periodic signals, presumably because the window is sampling different periods in both early and late intervals. In neither of those intervals is the 7.29-hr signal dominant, a result of limited and biased sampling of the signal. In the early interval the alias at 6.3 hr dominates. In the latter interval, the dominant 4.4 hr signal is *not* an alias of 7.29 hr and in fact no single period and its aliases can reproduce the full pattern of signals.

Based on such discrepancies, Fraser et al. (2017) proposed that 1I/‘Oumuamua is a non-principal axis (NPA) rotator and “tumbling”. They found that two periods of 7.4 and 7.9 hr (plotted as the solid blue lines in Fig. 2) can adequately, but perhaps not uniquely explain the data. These values can explain the short-period alias in the early interval, but not the 8.8 hr signal in the latter interval, except, perhaps if one invokes a 48 hr sampling alias. A different choice of 7.29 and 7.51 hr periods (solid purple lines) better explains the 6.3 and 8.8 hr signals, but not the (weaker) 8 hr signal. The 7.51 hr period is close to the 7.55 hr found by Drahus et al. (2017) in the late interval.

If NPA rotation occurs, changes in rotation period constrain the ratio of principal axes. Because angular momentum is conserved, the ratio of periods  $P_1/P_2$  is proportional to the ratio of principal moments of inertia  $I_1/I_2$ . In the case of an ellipsoidal geometry,  $P_1/P_2 = (a^2 + b^2)/(a^2 + c^2)$ , where rotation alternates between the  $b$  and  $c$  axes. When  $a \gg b, c$ , as has been proposed for 1I/‘Oumuamua,  $P_1/P_2 \approx 1 + (b^2 - c^2)/a^2$ . For such extremely elongated objects the

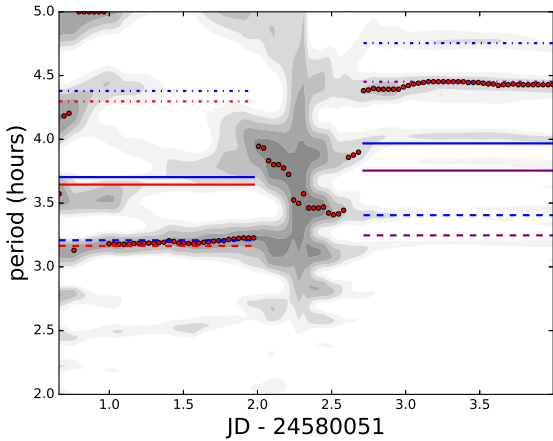


**Figure 2.** Periodogram power vs. time where the moving window is adjusted to always include 100 data points and time is calculated as the mean time of points in the window. Red points mark period of maximum power. The red line is the half-period corresponding to a rotation of 7.29 hr. Blue and purple solid lines are the rotation half-periods proposed by Fraser et al. (2017) and this work, respectively. Dashed lines with corresponding colors are the expected alias signals produced by 24-hr sampling.

long axis dominates the moment of inertia and the difference in periods is small. If  $a/b = 10$  and  $b \approx c$ , the difference is  $\ll 1\%$ , i.e. much less than 4 minutes. The difference in period implied by the observations is much larger. e.g. about 30 min (Fraser et al. 2017), 16 min (Drahus et al. 2017), or 13 min (this work). A difference of at least 3% indicates  $a/b < 5$ . Real asteroids are of course not perfectly ellipsoidal, but the scaling relationships still hold, the long axis will still force the difference in moments of inertia to be small, and deviations from the ellipsoid case will only modulate that difference in a minor way. For example, the difference between the individual principal moments of inertia of a cuboid is only 8% larger than that of an ellipsoid with the same volume and axis ratios.

Photometry of 1I/'Oumuamua phased to 7.29 hr are plotted in Fig. 3), showing the apparent amplitude  $\Delta m \approx 2.5$  (uncorrected for phase effects) which inspired aspect ratio estimates of  $a/b \approx 10$ . However, the amplitudes of asteroid lightcurves depends on phase angle in a manner that is a function of geometry and surface scattering properties (Gutiérrez et al. 2006, e.g.), and this effect must be included when estimating its shape (Fraser et al. 2017). To ascertain this, I calculated lightcurves using a finite-element model of a rotating ellipsoid having  $a > b = c$  and a uniform surface following either a Lambertian or Hapke scattering law including macroscopic roughness (Hapke 1993), and adopting the Earth-Sun-1I/'Oumuamua viewing geometry of 27 October 2017 (phase angle = 22 deg). The lightcurve amplitude  $\Delta m$  depends on the unknown rotational pole vector of 1I/'Oumuamua, but the maximum possible amplitude for a given  $a/b$  can be found by varying obliquity ( $\delta$ ) and longitude of the rotation axis with respect to the orbital apse line ( $\omega$ ).

Figure 4 plots  $\Delta m$  as a function of  $a/b$  and  $\omega$  for  $\delta = 30$  deg. Solid contours are for a Lambertian surface and dashed contours are for Hapke scattering with param-

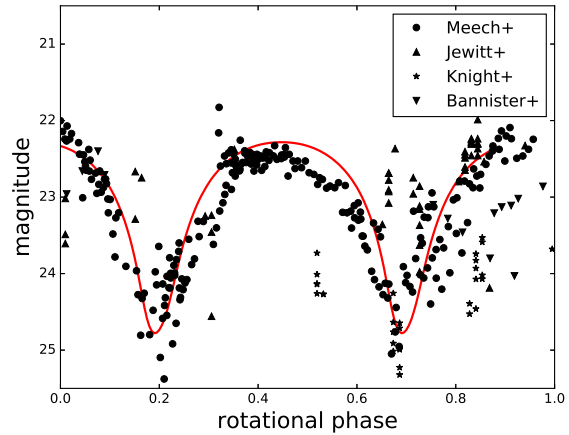


**Figure 3.** Lightcurve of 1I/'Oumuamua produced by phasing published photometry to a 7.29 hr period. The solid red curve is a model of a contact binary composed of equal-mass equilibrium prolate ellipsoids with non-uniform surfaces (Hapke-scattering except for dark Lambertian-scattering “caps” on the outer poles extending 57 deg to the equators, see text.) Arbitrary offsets of rotational phase and magnitude have been applied to the model.

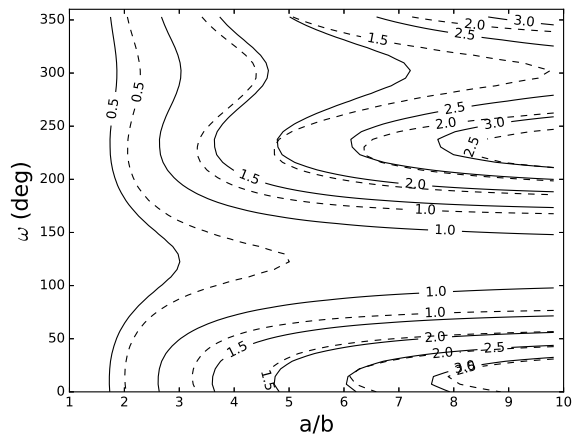


**Figure 4.** Rotational lightcurve amplitude (magnitudes) of a single prolate ellipsoid vs aspect ratio  $a/b$  ( $b = c$ ) and longitude of the rotation axis  $\omega$  with respect to the orbit apse, for the case of a Lambertian scattering surface (solid contours) and Hapke scattering with parameters of the average C-type asteroid (dashed contours). The rotational obliquity  $\delta$  is set to 30 deg.: varying  $\delta$  changes the dependence on  $\omega$  but largely not on  $a/b$ .

ter values characteristic of C-type asteroids (Li et al. 2015). The maximum  $\Delta m$  occurs when the object’s aspect angle (angle between the rotation axis and line of sight) is near 90 deg and is fairly insensitive to  $\delta$ , although the range of satisfactory values of  $\omega$  increases with decreasing  $\delta$ . With a Lambertian surface,  $\Delta m = 2.5$  can be produced for  $a/b$  as small as 6, but for that of a C-type asteroid, the minimum  $a/b = 8$ . (Average parameters for S- and V-type asteroids give similar results). Drahus et al. (2017) find a smaller lower limit of  $a/b = 4.63$ .

Large lightcurve amplitudes as well as the cusp-like minima seen in Fig. 3 are characteristic of binary asteroids where

one component eclipses the other twice a rotation/orbit. The possibility that 11/‘Oumuamua is a contact binary was considered and rejected by Meech et al. (2017) but revisited by Bannister et al. (2017). Contact binaries have representatives among all small body populations in the Solar System (e.g., Hudson et al. 1997; Margot et al. 2002; Marchis et al. 2006, 2014; Waszczak et al. 2015). Mechanisms that can produce such objects include spin-up and rotational disruption as a result of the Yarkovsky-O’Keefe-Radzievskii-Paddack (YORP) effect (Pravec & Harris 2007), tidal disruption during a close encounter with a planet (Morbidelli et al. 2006) or a collision (Paolicchi et al. 2002). The requirements of any of these mechanisms (proximity to a star, encounter with a planet, or collision with another body) are consistent with the scenario where 11/‘Oumuamua formed close to another star and was ejected by a planet (see Sec. 4).

A body formed as a result of disruption is expected to have very low intrinsic strength and its shape could closely follow an equipotential surface. This configuration can be approximated by a pair of Roche ellipsoids with axis ratios that depend on the mass-ratio of the components and the ratio of centripetal to gravitational forces  $\Omega^2/(\pi G\rho)$ , where  $\Omega = 2\pi/P$ ,  $G$  is the gravitational constant, and  $\rho$  is the mean density (Leone et al. 1984). The maximum axis ratio occurs at the Roche stability limit ( $a/b \approx 1.6$ ) where, for equal-mass components  $\rho \approx 2.1 \text{ g cm}^{-3} (P/7.3 \text{ hr})^{-2}$ . Many asteroids have this density or higher (Carry 2012). The axis ratio of each component of such a binary is about 1:0.62:0.56 (Leone et al. 1984). A contact binary can also tumble: For such an object the difference in periods would be 15 minutes.

Figure 5 is the same as Fig. 4, but 11/‘Oumuamua is modeled as a contact binary consisting of identical prolate ellipsoids aligned along the connecting axis. Bodies at the stability limit  $a/b \approx 1.7$  (vertical dashed-dot line) cannot reproduce the observed variability of 11/‘Oumuamua. Larger aspect ratios and greater variability are possible if the bodies have finite strength, i.e. a minimum  $\sim 1 \text{ Pa}$  (Meech et al. 2017; Bolin et al. 2017). For a Lambertian-scattering surface (solid contours in Fig. 5), a minimum ratio of  $a/b = 4.2$  is required to explain  $\Delta m = 2.5$  and thus an overall ratio of  $> 8.4$ ). Hapke scattering characteristic of a C-type asteroid (dashed contours, Li et al. 2015) requires still larger ( $\approx 10$ ) axis ratios. These values could conflict with the observation of significantly different periods during tumbling.

More modest axis ratios combined with surface reflectance variation can explain the lightcurve of 11/‘Oumuamua. In particular, if the outer poles of the bodies are much darker than the inward-facing surfaces, the axis ratios can be consistent with an equilibrium ellipsoid. Figure 6 plots  $\Delta m$  vs. the angular size of the dark end-caps (as measured from the poles). The surface of the caps is modeled as a Lambertian scatterer with albedo of 0.03 and the remaining surface as a Hapke scatterer with the parameters of a relatively bright E-type asteroid (Li et al. 2015, geometric albedo = 0.34). Such extreme (factor of 10) albedo variation has not been observed for any Solar System asteroid, but is comparable to that of Pluto and the Saturnian satellite Iapetus. A dark region extending 60 deg from the outer poles of the surface will generate the observed variability (Fig. 6 and red curve in Fig. 3). Differences between the observations from the model are most likely due to the

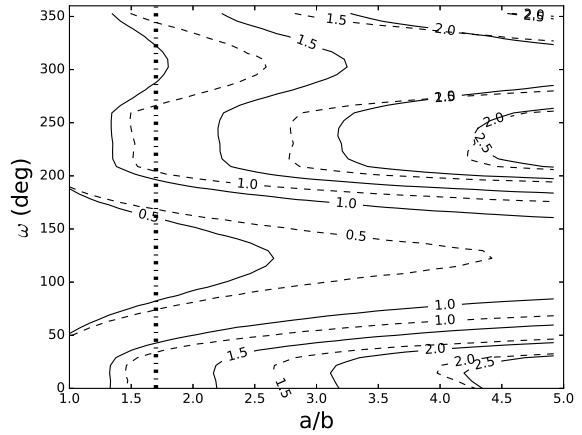


**Figure 5.** Rotational lightcurve amplitude (magnitudes) of a contact binary consisting of two identical prolate ellipsoids vs. individual aspect ratio  $a/b$  ( $b = c$ ) and longitude of the rotation axis  $\omega$  with respect to the orbit apse, for the case of a Lambertian scattering surface (solid contours) and Hapke scattering with parameters of the average C-type asteroid (dashed contours). The rotational obliquity  $\delta$  is set to 30 deg.: varying  $\delta$  changes the dependence on  $\omega$  but largely not on  $a/b$ . The vertical line is the expected axis ratio of a Roche ellipsoid at the stability limit.

departures of the object’s shape from a pair of ellipsoids and more complex variations in albedo than considered here.

One reason the albedo could be non-uniform is a partial mantle of brighter dust covering a darker surface. The latter is absent where the net surface acceleration (gravity minus centripetal force) is weakest, i.e. at the outward-facing poles of the components<sup>1</sup> Although the reflectance spectra of the two different surfaces may differ markedly, this might not be apparent in a low signal-to-noise spectrum since the signal from the brighter surface component dominates.

### 3 ORIGIN OF 11/‘Oumuamua

The radiant point of 11/‘Oumuamua (near 15h48m +34d01’) is only 8 deg. from the Solar apex, reflecting its low “peculiar” velocity with respect to the Local Standard of Rest (LSR). Molecular clouds and newly formed stars largely move with the LSR, but as stars age their peculiar velocities increase as roughly  $t^{1/2}$  due to scattering by other clouds and asymmetries in the Galactic potential such as spiral arms (Aumer et al. 2016, e.g.); this is the basis of the kinematic method of estimating stellar ages. Also, coeval groups of stars spawned by the same cloud initially share a common space motion ( $UVW$ ) this can be used to identify members of these associations for up to hundreds of Myr, long after they have spatially dispersed (e.g., Gagné et al. 2018).

The pre-encounter space motion of 11/‘Oumuamua ( $UVW = -11.440 \pm 0.009, -22.377 \pm 0.009, -7.743 \pm 0.010 \text{ km s}^{-1}$ ) and its peculiar motion is  $9 \text{ km s}^{-1}$  with respect to the LSR (Coşkunoglu et al. 2011), much less than

<sup>1</sup> Although the shape of a strengthless body can relax to an equipotential surface, the net acceleration at the surface – the vertical gradient of the potential – will vary.

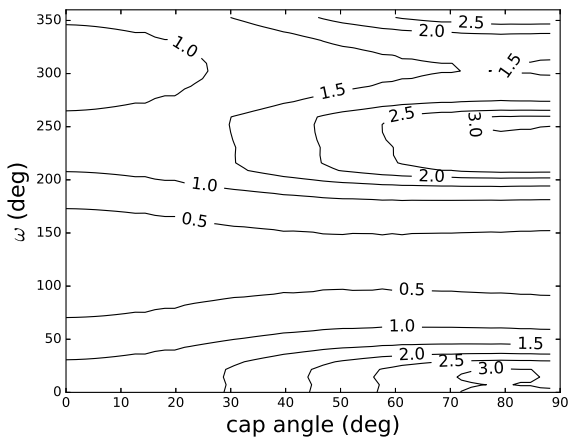


**Figure 6.** Rotational lightcurve amplitude (magnitudes) of a contact binary consisting of two Roche ellipsoids  $a/b = 1.7$  ( $b = c$ ) with end-caps of C-type scattering surfaces and brighter E-type asteroid-like material over the remainder. The axes are the angle subtended by the caps relative to the outer poles of the ellipsoids and the longitude  $\omega$  of the rotation axis with respect to the orbit apse, a proxy for the aspect angle. The obliquity is fixed at  $\delta = 30$  deg.

the  $50 \text{ km s}^{-1}$  velocity dispersion of nearby stars in the Galactic disk (Anguiano et al. 2017). Most of this  $9 \text{ km s}^{-1}$  is in the direction of Galactic rotation ( $V$ ) where the uncertainty in LSR motion is largest.<sup>2</sup> Based on this, Gaidos et al. (2017) and Feng & Jones (2018) suggested that the formation (or at least ejection) age of 1I/'Oumuamua is young compared to stars in the Solar neighborhood<sup>3</sup> Moreover, the space motion of 1I/'Oumuamua is within  $1\text{-}2 \text{ km s}^{-1}$  of that of the 40-50 Myr-old Carina and Columba stellar associations, leading Gaidos et al. (2017) to suggest an origin around a star in a member of these associations and ejection sometime after 40-50 Myr ago. An object moving at  $1\text{-}2 \text{ km s}^{-1}$  would cover the distance to these clusters ( $\approx 50 \text{ pc}$ ) in under 50 Myr.

However, the correlation between the kinematics of stars (and ejected planetesimals) and age is only a *statistical* relation and, like old stars, 1I/'Oumuamua could have a low peculiar motion close to that of a young stellar association by coincidence. A frequentist calculation of the probability of this null hypothesis is:

$$p = \frac{d_u d_v d_w}{\sigma_u \sigma_v \sigma_w} \sum_i \exp[-\Delta \vec{v}_i \mathbf{D} \Delta \vec{v}_i / 2], \quad (1)$$

where  $\mathbf{D}$  is the inverse of the velocity dispersion matrix of the cluster,  $\Delta \vec{v}_i$  is the relative velocity of the  $i$ th association with respect to the local standard of rest (Coşkunoglu et al. 2011),  $d$  are the principal components of  $\mathbf{D}$ , and  $\sigma$  the velocity dispersion components of the thin disk (Anguiano et al. 2017). (Errors in the space motion

of 1I/'Oumuamua are  $10 \text{ m s}^{-1}$  and can be neglected.) The associations included in the summation are TW Hydra,  $\beta$  Pictoris, Tucana-Horologium, Columba, Carina, Argus, and AB Doradus (from Gagné et al. 2014),  $\sigma_{32}$  Orionis (Bell et al. 2017),  $\epsilon$  and  $\eta$  Chamaeleontis (Mamajek et al. 1999; Murphy et al. 2013), Octans (Torres et al. 2008),  $\alpha$  Persei (Makarov 2006), the  $\rho$  Ophiucus and Upper Scorpius star-forming regions (Dahm et al. 2012; Cook et al. 2017) and the Pleiades (Galli et al. 2017). The total probability is 0.4%. Although this is a lower limit, since there may be undiscovered nearby associations, the probability that the young association-like motion of 1I/'Oumuamua is a coincidence is very likely  $< 1\%$ . The space motion of the source association will not exactly equal that of 1I/'Oumuamua because of stellar velocity dispersion (typically  $\sim 1 \text{ km s}^{-1}$ ) and a finite ejection velocity; either that latter is also small, or the association-like motion of 1I/'Oumuamua is a low-probability coincidence.

A more rigorous test of common origin would be to dynamically track the *spatial* locations of both 1I/'Oumuamua and an association back in time to some epoch to where they coincide. This is difficult because associations are often dispersed over tens of pc, their centers are not well determined, and the member stars could have had a finite velocity dispersion at the epoch of ejection. Moreover, errors in position due to errors in velocity and perturbations by field stars *accumulate* as  $t^{3/2}$  to pc-scale errors in  $\sim 100 \text{ Myr}$  (Zhang 2018). Figure 7 shows the results of track-back simulations for the different moving groups using the gravitational potential of (Irrgang et al. 2013). The positions of the associations with respect to 1I/'Oumuamua in the rotating frame of the LSR are plotted as  $r \equiv \sqrt{x^2 + y^2}$  and  $z$ , where  $x, y, z$  are towards the Galactic center, direction of Galactic rotation, North Galactic Pole, respectively. The tracks end at the estimated formation time of each association/cluster. A potential origin would have a track that passed through or near the origin at the epoch of ejection. The current physical sizes of the associations are indicated by the ellipses in Fig. 7, but this does not include the spatial extent corresponding to the accumulation of velocity uncertainty with time.

No unambiguous candidate for the birthplace of 1I/'Oumuamua emerges from this analysis. 1I/'Oumuamua is still *approaching*, not moving away from, the Carina, Columba, and Tucana-Horologium clusters all of which have similar space motions. 1I/'Oumuamua – and the Sun – are currently encountering the margins of the AB Doradus and  $\beta$  Pictoris associations but the velocity differences are 9 and 7  $\text{km s}^{-1}$ , respectively. For the orbits of Carina and 1I/'Oumuamua to meet in the past the association's  $v$  must be changed by 4  $\text{km s}^{-1}$  and its  $w$  by 3.2  $\text{km s}^{-1}$ , something excluded by measurement precision. Alternatively, a hypothetical association with the space motion of Carina but at a different current location could be the source. A range of  $xyz$  values are possible given the proportionally large uncertainty in the relative velocity between 1I/'Oumuamua and Carina and the dependence on the epoch of ejection, but one set is (29,6,82) pc, or 87 pc in the direction of  $\alpha = 212$  deg.,  $\delta = +19$  deg. (near the star Arcturus). The Coma Berenices association is near this location but has a very different  $UVW$  (Gagné et al. 2014).

<sup>2</sup> The Sun was likely 1I/'Oumuamua's first stellar encounter since ejection since the probability of approaching within 100 AU of any star in 5 Gyr is  $\lesssim 1\%$ .

<sup>3</sup> Statistically, 1I/'Oumuamua would have an equally high peculiar motion whether it was recently ejected from an old star or ejected long ago from a young star that is now equally old.

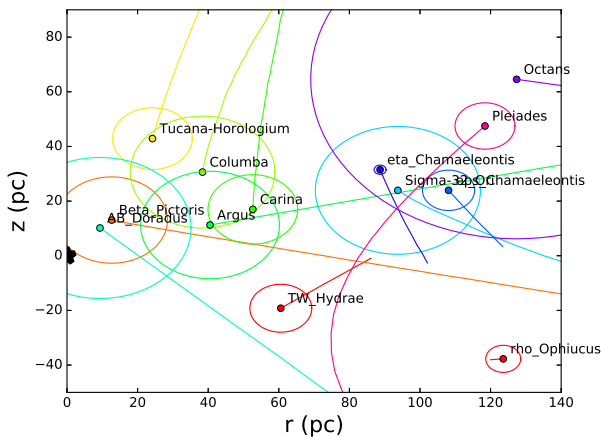


**Figure 7.** Plot of the relative motion of young stellar associations and clusters with respect to 1I/'Oumuamua (black star at origin) in  $r \equiv \sqrt{x^2 + y^2}$  vs  $z$  coordinates. Circular points indicate the current centers of the clusters/association, the ellipses indicate the approximate current size, and the trails indicate the motion back to the estimated time of association/cluster formation.

#### 4 DISCUSSION

1I/'Oumuamua almost certainly formed around another star and its detection implies a space density of similar objects corresponding to an ejected mass of a few  $M_{\oplus}$  per star (Gaidos et al. 2017; Trilling et al. 2017; Raymond et al. 2018). The circumstances and timing of 1I/'Oumuamua's formation and evolution in its home system, as well as the launch onto its interstellar voyage are not known, but 1I/'Oumuamua's shape, composition, and motion provide tantalizing hints.

Planetesimals are more likely to be ejected rather than accreted by a planet with an escape speed exceeding its orbital speed and thus more massive planets on wider orbits are likely to be responsible (Gaidos et al. 2017; Raymond et al. 2018). Also, planets that are migrating or excited onto highly eccentric orbits can eject larger numbers of planetesimals. The formation of a giant planet by rapid capture of a gas envelope, migration through (or with) the disk, and scattering by mutual gravitational perturbations are therefore potential major episodes of planetesimal ejection. Gas giant formation and migration occurs in  $\lesssim 10$  Myr (the typical disk lifetime) while orbital instability in two (giant) planet systems occur on a timescale that is a super-exponentially increasing function of separation from the nearest mean-motion resonance (Chatterjee et al. 2008, the existence of additional planets complicates this picture). Planetesimal ejection, averaged over many systems, is thus expected to peak within 10 Myr and decrease with time. This might be reflected in the decline in incidence of debris disks with age (Carpenter et al. 2009; Sierchio et al. 2014), if the dust is the product of collisions of planetesimals exited onto crossing orbits by giant planets.

Binaries, including contact binaries are one outcome of disruption of a minor body by Yarkovsky-O'Keefe-Radzievskii-Paddack (YORP) spin-up (Pravec & Harris 2007), tidal disruption during a close encounter with a planet (Bottke & Melosh 1996; Walsh & Richardson 2006) or a

collision with another minor body (Paolicchi et al. 2002). Radiation-driven (YORP) spin-up to the break-up rate requires at least  $\sim 1$  Myr of proximity to the host star, depending on mean distance and luminosity (Jacobson et al. 2014). The mean collision time among planetesimals in a disk is proportional to the characteristic size and inversely proportional to the surface density of solids, but for a minimum-mass nebula of 1 km bodies at 5 AU it is comparable to the ejection time ( $\sim 10^5$  yr) by a Jupiter-mass planet (Tremaine 1993). Disruption by tides is expected to be comparatively rare: Raymond et al. (2018) found that only 0.1-1% of ejected planetesimals in their simulations had previously passed within two Roche radii of a planet. However, tidal disruption of large ( $\sim 100$  km) bodies would produce many smaller objects that could dominate the ejecta population (see below).

In planetary systems with solar-like ratios of heavy elements, the amount of mass in condensible ices is about twice that in “rocks” (Lodders 2003). Since icy planetesimals form farther from a host star they are more likely to be ejected than their rocky inner counterparts, hence the expectation that most interstellar interlopers are icy (Raymond et al. 2018). 1I/'Oumuamua's surprising lack of detectable cometary activity despite a perihelion of 0.25 AU indicates lack of ices within 1 m of its surface, the predicted penetration depth of the thermal wave. Jewitt et al. (2017) and Fitzsimmons et al. (2017) proposed that Galactic cosmic rays depleted ices from this zone. But this mechanism is contradicted by long-period comets from the Oort Cloud, which experienced interstellar conditions at  $> 10,000$  AU for 4.5 Gyr but retain surface ices. Moreover, if 1I/'Oumuamua is composed of strengthless material filling critical Roche ellipsoids then its density is  $\approx 2$  g cm $^{-3}$ , also disfavoring significant ice content.

An ice-free 1I/'Oumuamua could be explained if ejected rocky planetesimals are more numerous, but are typically much smaller. The size distribution of Oort cloud comets flattens markedly below 2 km and is negligible below 500 m (Fernández & Sosa 2012). If the characteristic sizes for ejected rocky and icy planetesimals are 100 m (1I/'Oumuamua-like) and 1 km (comet-like), respectively, then the relative numbers would exceed 100:1. Differences in size distribution with ice content could arise from variation in the lifetime of disk gas, which promotes (re-)aggregation of smaller bodies, or more efficient collisional fragmentation of planetesimals collisions closer to the star (Kenyon & Bromley 2012). Raymond et al. (2018) link tidal disruption by a planet to the lack of ices in 1I/'Oumuamua by the desiccation that can occur if multiple star-approaching orbits follow tidal disruption but precede ejection. They propose that the rarity of such events among ejected planetesimals (0.1-1% in their simulations) is balanced by the shear number of fragments produced.

The age of 1I/'Oumuamua is not known: a pre-encounter velocity that is close to those of some young stellar associations with a false alarm probability  $< 1\%$  hints at a common origin and age of  $\lesssim 100$  Myr (Gaidos et al. 2017; Feng & Jones 2018) but track-back simulations are limited by the precision of available stellar space motions, the completeness of catalogs of nearby young stars, and the rapid accumulation of positional uncertainty with reversed time (Zhang 2018). The *Gaia* mission will provide a far more



**Table 1.** Dynamical Bias Ratios

Stellar Group	Bias at 1 AU <sup>a</sup>
Upper Scorpius	2.8
$\rho$ Ophiucus	2.3
Octans	2.2
Beta Pictoris Moving Group	1.7
TW Hydra Association	1.5
Tucana-Horologium	1.5
$\sigma_{32}$ Ori	1.4
Columba	1.3
Argus	1.3
Carina	1.3
$\epsilon$ Chamaeleontis	1.3
$\eta$ Chamaeleontis	1.2
$\alpha$ Persei	1.0
AB Doradus	0.9
Pleiades	0.9

<sup>a</sup>relative to the velocity distribution of the nearby Galactic disk.

complete and accurate inventory of nearby young associations and their dynamics (Moraux 2016), and perhaps resolution of this question.

A young age would create a conundrum: The average age of stars in the Galactic disk is a few Gyr and if each of these also produced planetesimals in roughly equal numbers, the prior probability that the first object we discover is much younger is very low. This discrepancy would have to be explained by strong (factor of  $\sim 100$ ) selection against older objects. Tidal disruption of planetesimals by a close encounter with a star is  $\sim 10^{-9}$  in 5 Gyr and disruptive spin-up by the YORP effect is inoperable beyond  $\sim 100$  AU for 100-m objects like 1I/‘Oumuamua (Jacobson et al. 2014). Mechanical torques could be important if the original object is sufficiently irregular, but only on a timescale of several 100 Myr (Hoang et al. 2018). Gravitational focusing provides a modest bias against older objects moving at higher speeds due to scattering by stars and molecular clouds. This bias is a factor  $1 + 2(v_{\text{orb}}/v_{\infty})^2$ , where  $v_{\text{orb}}$  is the orbital velocity at 1 AU and  $v_{\infty}$  is the planetesimal approach velocity. This factor was calculated for nearby young associations and clusters assuming that the space motions of young planetesimals were distributed like that of the stars in each parent moving group (Torres et al. 2008; Gagné et al. 2014), and the motions of older objects were distributed according to the velocity ellipsoid of the the Galactic thin disk Anguiano et al. (2017). Enhancements by at most 2-3 are predicted (Table 4), well short of what is required.

The surfaces of Main Belt asteroids become redder and darker from radiation and micrometeorite exposure (“space weathering”) in  $10^4 - 10^6$  yr (Brunetto et al. 2015), and an analogous process acting on interstellar objects could render them darker and undetectable as their surfaces age.<sup>4</sup> The interstellar flux of protons in the energy range (up to

a few keV) thought to be partly responsible space weathering is  $\lesssim 10^{-3}$  of the flux at 2.5 AU (Brunetto et al. 2015), but the flux of higher energy Galactic cosmic rays is many orders of magnitudes greater due to the absence of a Solar magnetic field (Cooper et al. 2003). Darkening could occur by loss of any brighter, scattering dust mantle, e.g. by electrostatic charging and levitation (Mendis et al. 1981; Lee 1996). This dust layer would not be replenished by micrometeorite impacts since the mass flux of impacting interstellar dust particles is at least 2-3 orders below that estimated in the inner Solar System (Altobelli et al. 2016; Bennett et al. 2013). The corollary of this explanation is that many more objects with older, darker surfaces enter the Solar System but remain undetected.

Drawing conclusion from a single object in a population is dangerous, especially because selection effects like those described above may influence a detection. The addition of a second telescope to the Pan-STARRS survey (Burgett 2012; Engelhardt et al. 2017) and the advent of the Large Synoptic Survey Telescope in 2021 (Moro-Martín et al. 2009; Cook et al. 2016) should provide meaningful constraints on the size, shape, and velocity distribution of interstellar planetesimals and, perhaps, insight into planetesimal growth and planet formation from a new perspective. If there is a strong detection bias towards young objects, many future detections will have radiants near the Solar apex.

A close-up investigation of an interstellar interloper like 1I/‘Oumuamua is clearly desirable, but a space mission to rendezvous (or collide) with one would be challenged by the high  $\Delta v$  required and the limited warning time. Any interstellar objects captured onto a bound orbit around the Sun by Jupiter (no other planet offers a comparable capture cross-section: Valtonen & Innanen 1982) would be a more accessible target of exploration. Based on a number density for extrasolar comets of  $\sim 10^{13}$  pc<sup>-3</sup>, Torbett (1986) estimated one capture per 60 Myr, much longer than the ejection by Jupiter (Levison & Duncan 1994, 450 kyr.). If the actual number density of 1I/‘Oumuamua-like objects is higher, the steady state number could be a few.

Alternatively, smaller interstellar objects could be numerous enough to occasionally strike Earth as meteorites. In the case of the -7/2 power-law distribution produced by a collisional cascade (O’Brien & Greenberg 2003), for every 1I/‘Oumuamua-size object that passes within 1 AU of the Sun, a sister 30-cm object collides with Earth. About 1000 objects of such size impact every year (Brown et al. 2002) and since there are about 1200 meteorite falls in world-wide collections (Krot et al. 2014), this statistic, subject to the assumption of a steep size distribution raises the possibility that one may be interstellar. No extrasolar meteorites have been identified, but two indicators of extrasolar origin are a primitive chondrite-like composition combined with a non-solar Pb-Pb radiometric age, and an oxygen isotopic composition that differs markedly from that of the Solar System (Clayton 1993) due to Galactic chemical evolution (Gaidos et al. 2009; Young et al. 2011).

## ACKNOWLEDGEMENTS

I thank Jeff Gillis-Davis, Paul Lucey, Sasha Krot, and Gary Huss for their advice and assistance, Wesley Fraser for pro-

<sup>4</sup> 1I/‘Oumuamua was only observable when it was close to both Earth and the Sun and would not have been detected had it been significantly fainter. For example, if it were entirely covered by a dark material and lacked the brighter midriff that could explain the rotational variability, its *peak* brightness would be 2.3 magnitudes fainter.

viding a fresh perspective on the manuscript, and a second, anonymous reviewer for helpful suggestions.

## REFERENCES

- Altobelli N., Postberg F., Fiege K., Trieloff M., Kimura H., Sterken V. J., Hsu H.-W., Hillier J., Khawaja N., Moragas-Klostermeyer G., Blum J., Burton M., Srama R., Kempf S., Gruen E., 2016, *Science*, 352, 312
- Anguiano B., Majewski S. R., Freeman K. C., Mitschang A. W., Smith M. C., 2017, *ArXiv e-prints*
- Aumer M., Binney J., Schönrich R., 2016, *MNRAS*, 462, 1697
- Bannister M. T., Schwamb M. E., Fraser W. C., Marsset M., Fitzsimmons A., Benecchi S. D., Lacerda P., Pike R. E., Kavelaars J. J., Smith A. B., Stewart S. O., Wang S.-Y., Lehner M. J., 2017, *ArXiv e-prints*
- Bell C. P. M., Murphy S. J., Mamajek E. E., 2017, *MNRAS*, 468, 1198
- Bennett C. J., Pirim C., Orlando T. M., 2013, *Chemical Reviews*, 113, 9086
- Bolin B. T., Weaver H. A., Fernandez Y. R., Lisse C. M., Huppenkothen D., Jones R. L., Juric M., Moeyens J., Schambeau C. A., Slater C. T., Ivezić Z., Connolly A. J., 2017, *ArXiv e-prints*
- Bottke Jr. W. F., Melosh H. J., 1996, *Icarus*, 124, 372
- Brown P., Spalding R. E., ReVelle D. O., Tagliaferri E., Worden S. P., 2002, *Nature*, 420, 294
- Brunetto R., Loeffler M. J., Nesvorný D., Sasaki S., Strazzulla G., 2015, *Asteroid Surface Alteration by Space Weathering Processes*. pp 597–616
- Burgett W. S., 2012, in *Modeling, Systems Engineering, and Project Management for Astronomy V* Vol. 8449 of *Proc. SPIE*, PS2: managing the next step in the Pan-STARRS wide field survey system. p. 84490T
- Carpenter J. M., Bouwman J., Mamajek E. E., Meyer M. R., Hillenbrand L. A., Backman D. E., Henning T., Hines D. C., Hollenbach D., Kim J. S., Moro-Martín A., Pascucci I., Silverstone M. D., Stauffer J. R., Wolf S., 2009, *ApJS*, 181, 197
- Carry B., 2012, *Planet. Space Sci.*, 73, 98
- Chatterjee S., Ford E. B., Matsumura S., Rasio F. A., 2008, *ApJ*, 686, 580
- Clayton R. N., 1993, *Annual Review of Earth and Planetary Sciences*, 21, 115
- Cook N. J., Scholz A., Jayawardhana R., 2017, *AJ*, 154, 256
- Cook N. V., Ragozzine D., Granvik M., Stephens D. C., 2016, *ApJ*, 825, 51
- Cooper J. F., Christian E. R., Richardson J. D., Wang C., 2003, *Earth Moon and Planets*, 92, 261
- Coşkunoglu B., Ak S., Bilir S., Karaali S., Yaz E., Gilmore G., Seabroke G. M., Bienaymé O., Bland-Hawthorn J., Campbell R., Freeman K. C., Gibson B., Grebel E. K., Munari U., Navarro J. F., Parker Q. A., 2011, *MNRAS*, 412, 1237
- Dahm S. E., Slesnick C. L., White R. J., 2012, *ApJ*, 745, 56
- Drahus M., Guzik P., Waniak W., Handzlik B., Kurowski S., Xu S., 2017, *ArXiv e-prints*
- Engelhardt T., Jedicke R., Vereš P., Fitzsimmons A., Deneau L., Beshore E., Meinke B., 2017, *AJ*, 153, 133
- Feng F., Jones H. R. A., 2018, *ApJ*, 852, L27
- Fernández J. A., Sosa A., 2012, *MNRAS*, 423, 1674
- Fitzsimmons A., Snodgrass C., Rozitis B., Yang B., Hyland



- M., Seccull T., Bannister M. T., Fraser W. C., Jedicke R., Lacerda P., 2017, ArXiv e-prints
- Fraser W. C., Pravec P., Fitzsimmons A., Lacerda P., Bannister M. T., Snodgrass C., Smolič I., 2017, ArXiv e-prints
- Gagné J., Lafrenière D., Doyon R., Malo L., Artigau É., 2014, ApJ, 783, 121
- Gagné J., Mamajek E. E., Malo L., Riedel A., Rodriguez D., Lafrenière D., Faherty J. K., Roy-Loubier O., Pueyo L., Robin A. C., Doyon R., 2018, ArXiv e-prints
- Gaidos E., Krot A. N., Huss G. R., 2009, ApJ, 705, L163
- Gaidos E., Williams J., Kraus A., 2017, Research Notes of the American Astronomical Society, 1, 13
- Galli P. A. B., Moraux E., Bouy H., Bouvier J., Olivares J., Teixeira R., 2017, A&A, 598, A48
- Gutiérrez P. J., Davidsson B. J. R., Ortiz J. L., Rodrigo R., Vidal-Núñez M. J., 2006, A&A, 454, 367
- Hansen B., Zuckerman B., 2017, Research Notes of the American Astronomical Society, 1, 55
- Hapke B., 1993, Theory of reflectance and emittance spectroscopy
- Hoang T., Loeb A., Lazarian A., Cho J., 2018, ArXiv e-prints
- Hudson R. S., Ostro S. J., Harris A. W., 1997, Icarus, 130, 165
- Irrgang A., Wilcox B., Tucker E., Schiefelbein L., 2013, A&A, 549, A137
- Jacobson S. A., Marzari F., Rossi A., Scheeres D. J., Davis D. R., 2014, MNRAS, 439, L95
- Jewitt D., Luu J., Rajagopal J., Kotulla R., Ridgway S., Liu W., Augusteijn T., 2017, ArXiv e-prints
- Jordi K., Grebel E. K., Ammon K., 2006, A&A, 460, 339
- Kenyon S. J., Bromley B. C., 2012, AJ, 143, 63
- Knight M. M., Protopapa S., Kelley M. S. P., Farnham T. L., Bauer J. M., Bodewits D., Feaga L. M., Sunshine J. M., 2017, ArXiv e-prints
- Krot A. N., Keil K., Scott E. R. D., Goodrich C. A., Weisberg M. K., 2014, Classification of Meteorites and Their Genetic Relationships. pp 1–63
- Lee P., 1996, Icarus, 124, 181
- Leone G., Paolicchi P., Farinella P., Zappala V., 1984, A&A, 140, 265
- Levison H. F., Duncan M. J., 1994, Icarus, 108, 18
- Li J.-Y., Helfenstein P., Buratti B., Takir D., Clark B. E., 2015, Asteroid Photometry. pp 129–150
- Lodders K., 2003, ApJ, 591, 1220
- Makarov V. V., 2006, AJ, 131, 2967
- Mamajek E., 2017, Research Notes of the American Astronomical Society, 1, 21
- Mamajek E. E., Lawson W. A., Feigelson E. D., 1999, ApJ, 516, L77
- Marchis F., Durech J., Castillo-Rogez J., Vachier F., Cuk M., Berthier J., Wong M. H., Kalas P., Duchene G., van Dam M. A., Hamanowa H., Viikinkoski M., 2014, ApJ, 783, L37
- Marchis F., Kaasalainen M., Hom E. F. Y., Berthier J., Enriquez J., Hestroffer D., Le Mignant D., de Pater I., 2006, Icarus, 185, 39
- Margot J. L., Nolan M. C., Benner L. A. M., Ostro S. J., Jurgens R. F., Giorgini J. D., Slade M. A., Campbell D. B., 2002, Science, 296, 1445
- Meech K. M., Weryk R., Micheli M., Kleyna J. T., Hainaut O. R., Jedicke R., Wainscoat R. J., Chambers K. C., Keane J. V., Petric A., Denneau L., Magnier E., Berger T., Huber M. E., Flewelling H., Waters C., Schunova-Lilly E., Chastel S., 2017, Nature, online
- Mendis D. A., Hill J. R., Houppis H. L. F., Whipple E. C., 1981, ApJ, 249, 787
- Moraux E., 2016, in Moraux E., Lebreton Y., Charbonnel C., eds, EAS Publications Series Vol. 80 of EAS Publications Series, Open clusters and associations in the Gaia era. pp 73–114
- Morbidelli A., Levison H. F., Bottke W. F., 2006, Meteoritics and Planetary Science, 41, 875
- Moro-Martín A., Turner E. L., Loeb A., 2009, ApJ, 704, 733
- Murphy S. J., Lawson W. A., Bessell M. S., 2013, MNRAS, 435, 1325
- O'Brien D. P., Greenberg R., 2003, Icarus, 164, 334
- Paolicchi P., Burns J. A., Weidenschilling S. J., 2002, Side Effects of Collisions: Spin Rate Changes, Tumbling Rotation States, and Binary Asteroids. pp 517–526
- Pravec P., Harris A. W., 2007, Icarus, 190, 250
- Rafikov R. R., 2018, ArXiv e-prints
- Raymond S. N., Armitage P. J., Veras D., 2018, ArXiv e-prints
- Raymond S. N., Veras D., Armitage P. J., Barclay T., Quintana E., 2018, MNRAS
- Scargle J. D., 1982, ApJ, 263, 835
- Sierchio J. M., Rieke G. H., Su K. Y. L., Gáspár A., 2014, ApJ, 785, 33
- Torbett M. V., 1986, AJ, 92, 171
- Torres C. A. O., Quast G. R., Melo C. H. F., Sterzik M. F., 2008, Young Nearby Loose Associations. p. 757
- Tremaine S., 1993, in Phillips J. A., Thorsett S. E., Kulkarni S. R., eds, Planets Around Pulsars Vol. 36 of Astronomical Society of the Pacific Conference Series, The distribution of comets around stars. pp 335–344
- Trilling D. E., Robinson T., Roegge A., Chandler C. O., Smith N., Loeffler M., Trujillo C., Navarro-Meza S., Glaspie L. M., 2017, ArXiv e-prints
- Valtonen M. J., Innanen K. A., 1982, ApJ, 255, 307
- Walsh K. J., Jacobson S. A., 2015, Formation and Evolution of Binary Asteroids. pp 375–393
- Walsh K. J., Richardson D. C., 2006, Icarus, 180, 201
- Waszczak A., Chang C.-K., Ofek E. O., Laher R., Masci F., Levitan D., Surace J., Cheng Y.-C., Ip W.-H., Kinoshita D., Helou G., Prince T. A., Kulkarni S., 2015, AJ, 150, 75
- Ye Q.-Z., Zhang Q., Kelley M. S. P., Brown P. G., 2017, ArXiv e-prints
- Young E. D., Gounelle M., Smith R. L., Morris M. R., Pontoppidan K. M., 2011, ApJ, 729, 43
- Zhang Q., 2018, ApJ, 852, L13